Portland State University
PDXScholar

Chemistry Faculty Publications and Presentations   Chemistry

10-2000

Structure and Phase Transitions of the 6, 6-Cyclopropane Isomer of C_{61}H_{2}

M. R. Stetzer
University of Pennsylvania

Paul A. Heiney
University of Pennsylvania

Peter W. Stephens
State University of New York at Stony Brook

R. E. Dinnebier
State University of New York at Stony Brook

Q. Zhu
Brookhaven National Laboratory

See next page for additional authors

Let us know how access to this document benefits you.

Follow this and additional works at: http://pdxscholar.library.pdx.edu/chem_fac

Part of the Chemistry Commons

Citation Details

Authors

M. R. Stetzer, Paul A. Heiney, Peter W. Stephens, R. E. Dinnebier, Q. Zhu, Andrew R. McGhie, Robert M. Strongin, B. M. Brandt, and Amos B. Smith III

Structure and phase transitions of the 6,6-cyclopropane isomer of $C_{61}H_2$

M. R. Stetzer* and P. A. Heiney[†]

Department of Physics and Astronomy and Laboratory for Research on the Structure of Matter,
University of Pennsylvania, Philadelphia, Pennsylvania 19104

P. W. Stephens and R. E. Dinnebier[‡]

Department of Physics and Astronomy, State University of New York at Stony Brook, Stony Brook, New York 11974

Q. Zhu[§]

Department of Physics, Brookhaven National Laboratory, Upton, New York 11973

A. R. McGhie

Laboratory for Research on the Structure of Matter, University of Pennsylvania, Philadelphia, Pennsylvania 19104

R. M. Strongin,** B. M. Brandt, and A. B. Smith III

Department of Chemistry and Laboratory for Research on the Structure of Matter,
University of Pennsylvania, Philadelphia, Pennsylvania 19104

(Received 22 May 2000)

We have used x-ray powder diffraction and differential scanning calorimetry to study the crystalline structures and thermal behavior of the 6,6-cyclopropane isomer of $C_{61}H_2$. At room temperature, the $C_{61}H_2$ cyclopropane molecules, like those of the 6,5-annulene isomer and $C_{60}O$ epoxide, are orientationally disordered and crystallize on a face-centered-cubic lattice such that their methylene groups are statistically disordered among the octahedral voids. *Unlike* 6,5-$C_{61}H_2$ and $C_{60}O$, the low-temperature structure is not $Pa\bar{3}$, but rather a low-symmetry orthorhombic lattice in which $a \approx b < c$. The orientational melting takes place via a two-step transition centered around 198–213 K.

I. INTRODUCTION

Simple derivatives of C_{60} (or [60]fullerene) offer unique model systems to study the effect of small molecular perturbations on crystal structure. Pristine C_{60} has the form of a spherical shell, with 60 symmetrically equivalent carbon atoms. At high temperatures, C_{60} forms an orientationally disordered face-centered-cubic (fcc) crystal[1,2] with $Fm\bar{3}m$ symmetry. At $T_C = 260$ K, solid C_{60} experiences a first-order phase transition into an orientationally ordered[2–5] simple cubic (sc) phase with $Pa\bar{3}$ symmetry and four molecules per unit cell.[3,4] The low-temperature phase continues to incorporate a substantial degree of both static and dynamic orientational disorder.[2,6–8] This transition, and the structures of the high- and low-temperature phases, have been the objects of numerous experimental and theoretical studies.[5,9,10]

The ordering transition is primarily driven by Coulombic interactions and angular contributions to the intermolecular van der Waals interactions, both arising from slight deviations from spherical symmetry intrinsic to the truncated icosahedral carbon cage.[7,11,12] Hence one might expect that the ordering transition itself would provide an excellent opportunity to examine small molecular deviations from spherical symmetry in various C_{60} derivatives, since the mechanisms which drive this transition are directly dependent upon the nonspherical components of the molecular architecture. The relatively modest perturbation of the C_{60} molecule resulting from the addition of a small group to the carbon cage can lead to compounds with solid-state characteristics qualitatively similar to those of C_{60} itself.

In the case of $C_{60}O$ epoxide,[13] a C_{60} derivative in which a single oxygen atom is added to the cage across what was formerly a carbon-carbon double bond, the high-temperature orientationally disordered phase is still characterized by an fcc structure with $Fm\bar{3}m$ symmetry, but each molecule is cylindrically disordered about the oxygen axis. This axis ratchets between the various octahedral and tetrahedral voids, with an approximately 66% occupancy of the larger octahedral voids.[14,15] The onset of the ordering transition, as determined by differential scanning calorimetry, occurs at 278 K, which is slightly higher than the onset temperature of 260 K in pristine C_{60} and is consistent with the decreased entropy of the high-temperature phase. The low-temperature phase is once again $Pa\bar{3}$, with the additional requirement that the epoxide moieties must be statistically disordered among the available voids.[14,15]

Similar effects are seen in some C_{60} intercalation compounds. Although cage rotation is almost completely suppressed in the alkali intercalates that are responsible for superconductivity,[10] the low- and high-temperature structures of $(CO)_xC_{60}$ are almost identical to those of pristine C_{60}, with the CO molecules confined to the octahedral voids.[16,17]

A slightly larger perturbation of the pristine C_{60} molecular architecture may be achieved via the addition of a methylene group to the carbon cage, since the CH_2 group extends far-
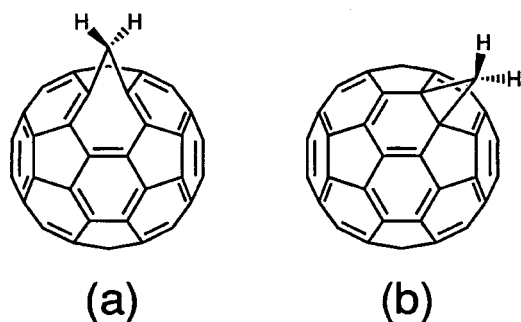
FIG. 1. The two isomers of $C_{61}H_2$. In the 6,5-annulene isomer (a), the methylene group replaces a carbon-carbon single bond shared by a hexagon and a pentagon. In the 6,6-cyclopropane isomer (b), the methylene group forms a three-membered ring at what was formerly a carbon-carbon double bond residing between two hexagons.

ther from the surface of the cage and occupies more volume than the epoxide moiety in $C_{60}O$. The 6,5-annulene and the 6,6-cyclopropane isomers of $C_{61}H_2$ are shown in Fig. 1. In the 6,5-annulene isomer,[18,19] the methylene group bridges what was formerly a carbon-carbon single bond shared by a hexagon and a pentagon on the carbon cage, while the hexagon and pentagon fuse into a single nine-membered ring. The 6,6-cyclopropane isomer,[19] on the other hand, results from the addition of the methylene unit to the carbon cage across what was a carbon-carbon double bond shared by two cage hexagons; in this isomer, a closed, three-membered ring links the methylene to the two bridge-head carbons.[19,20]

In the high-temperature fcc phase of the 6,5-annulene isomer of $C_{61}H_2$, the molecules are once again cylindrically disordered as in $C_{60}O$ epoxide, but the methylene groups are additionally constrained to occupy only the larger octahedral voids as a result of the considerable steric contributions arising from the group's hydrogen atoms.[21–24] The higher ordering transition onset temperature of 290 K is consistent with the significantly lower entropy of the high-temperature phase arising from the increased constraints on the orientation of the methylene axis. In the low-temperature orientationally ordered $Pa\bar{3}$ phase of 6,5-annulene $C_{61}H_2$, the methylene groups are once again statistically disordered among the larger octahedral voids.[21–24]

Presumably, as the side groups become larger and the perturbations of the molecular architecture become increasingly significant, deviations from pristine C_{60} behavior should become much more dramatic, and, beyond a certain point, the derivative compounds should become orientationally ordered at all temperatures, as is observed[25,26] in $C_{60}(OsO_4)(4-tert\text{-butylpyridine})_2$.

To address this issue, we[27] have examined the solid-state structures and thermal behavior of the 6,6-cyclopropane isomer of $C_{61}H_2$ using x-ray powder diffraction (XRPD) and differential scanning calorimetry (DSC). Density-functional calculations performed by Curioni *et al.*[28] suggest that the distance from the center of the carbon cage to the methylene carbon, which we shall refer to as the methylene radius, is approximately 0.2 Å larger in the cyclopropane isomer than it is in the annulene. This small increase in the methylene radius implies that the CH_2 group should extend farther into the voids, thus increasing the rotational hindrance arising

from tightened steric constraints. One might anticipate a decrease in the librational motion of the cage or possibly even a shift from true uniaxial rotation to static statistical disorder about the methylene axis. Additional deviations may arise from the different molecular symmetries of the two isomers. The question therefore is whether the energetic, steric, or symmetry differences arising from the attachment of the methylene group onto the carbon cage in a 6,6-cyclopropane configuration as opposed to the 6,5-annulene configuration are significant enough to make alternative solid-state structures and phase behavior possible or favorable.

The remainder of this paper will proceed as follows. In Sec. II, we will discuss the experimental techniques employed and the analysis of the x-ray data. Sections III, IV, and V discuss the high-temperature, low-temperature, and phase-transition properties of 6,6-cyclopropane $C_{61}H_2$, respectively. Finally, in Sec. VI we summarize our key results.

II. EXPERIMENT

Approximately 25 mg of 6,6-cyclopropane $C_{61}H_2$ were synthesized as previously described.[19] Residual solvent is known to play an important role in the structure and phase transitions of C_{60} and its derivatives.[5,29–33] To address this issue, the sample was heated under a dynamic vacuum of 10^{-7} Torr for 29 h at a temperature between 347 and 355 K, 19 h at 383 K, and 46 h at a temperature between 418 and 423 K. This heating protocol was designed to remove as much solvent as possible without thermally degrading the sample. After drying, samples were stored in a glovebox under inert argon atmosphere. The glass vials were wrapped in aluminum foil to minimize exposure to light.

Thermal properties were determined using a TA Instruments DSC 2920 apparatus. This instrument incorporates a single heating/cooling block for both the sample and reference,[34] and acts as a Boersma differential thermal analyzer.[35] Heat flow and other calorimetric information were extracted from the raw ΔT using experimentally determined calibration constants.[36] For a typical measurement, 5–6 mg of powdered material were placed in crimped aluminum pans under a standard air environment. An identical empty pan was used as a reference. The enthalpy change, ΔH, for any transitions was determined by interpolating a linear baseline in the immediate vicinity of the endo- or exotherm, and then calculating the area enclosed between the baseline and the feature of interest. The onset temperature was obtained by extrapolating the linear portion of the onset curve to the point where it intersected the linear baseline.

For XRPD measurements, samples were loaded in glass capillaries using a "piston" technique,[15,27] in which the sample was deposited in a 1-mm glass capillary and a second capillary was inserted into the first, compressing the sample and removing any large voids. Both capillaries were then sealed with a torch when possible, although in some cases the capillaries were sealed with epoxy in the glovebox. Low-temperature measurements were performed using Air Products Displex cryostats. The XRPD data were collected on Beamlines X7A and X3B1 at the National Synchrotron Light Source, Brookhaven National Laboratory.

For the measurements at Beamline X7A, a wavelength of 1.149 84 Å was selected via a channel-cut Si(111) mono-

chromator, and the intensity of the incoming beam was monitored using an ion chamber. Scattered radiation was then collected by a linear position sensitive detector (PSD) mounted on the 2θ arm of the diffractometer at a distance of ~ 1 m from the sample capillary.[37] The effective angular resolution was $\Delta 2\theta = 0.05 - 0.1°$. Full scans covering an angular range $4 \leq 2\theta \leq 71°$ (or $0.38 \leq Q \leq 6.35$ Å^{-1}) were performed at selected temperatures, and scans over a smaller range $0.95 \leq Q \leq 4.27$ Å^{-1} were systematically carried out at many temperatures. To improve powder averaging, the capillary was rotated slightly about its axis (perpendicular to the scattering plane) by incorporating a continuous $5°$ θ oscillation into the scan. We used a step size of $1°$ and collected data from the central $2°$ of the PSD, ensuring overlap between adjacent points. PSD data collected at X7A were binned, corrected for nonlinearities, normalized, and merged into data sets consisting of intensity *versus* angle.

The measurements at X3B1 were done in a triple-axis configuration. The incident wavelength $\lambda = 1.149\,15 \pm 0.000\,05$ Å was selected via an Si(111) monochromator. The diffracted radiation was then detected using a Ge(111) analyzer crystal and a NaI scintillation counter. The experimental data were corrected for detector deadtime (≈ 3 μs) and normalized to a synchrotron ring current of 100 mA. The instrumental resolution was $\Delta 2\theta = 0.015 - 0.03°$. These measurements employed a 1-mm capillary sealed with epoxy. Data were collected with $3 \leq 2\theta \leq 25°$ ($0.286 \leq Q \leq 2.367$ Å^{-1}) in steps of $0.005°$, counting for three seconds per point, and in a second range of $25 \leq 2\theta \leq 56°$ ($2.367 \leq Q \leq 5.165$ Å^{-1}) in steps of $0.005°$, counting for six seconds per point.

The resultant XRPD data sets were analyzed either by least-squares fits to the integrated intensities of peaks derived from pattern decomposition, or by a (more time-consuming) Rietveld analysis.

In the first approach, integrated intensities were extracted from a given XRPD pattern via least-squares fits of the raw profiles to empirical peak shapes. Separate portions of the full powder pattern were analyzed independently such that one or two peaks were fitted at a time using a linear background term and the appropriate number of peaks. The empirical peak shape chosen was a weighted sum of a Gaussian and an asymmetric Lorentzian. Error bars for the integrated intensity were obtained by systematically increasing and then decreasing each peak's fitted intensity with respect to the best-fit value until a 10% increase in χ^2 was observed (for single-peak fits) or 5% per peak in multiple-peak fits. The $\{111\}$ reflection was omitted from the refinements, since the intensity, position, and peak shape of the $\{111\}$ reflection in C_{60} and its derivatives may all be altered significantly by the presence of stacking faults within the compounds.[14–16,38–40]

The lattice parameters were obtained via an independent LeBail fit[37,41] on the full powder pattern, using GSAS (General Structure Analysis System).[42] After satisfactory lattice parameters were obtained, these values were fixed and treated as known constants in our integrated intensity refinement code. The quality of fit was evaluated using the χ^2 goodness-of-fit parameter,[43] the Bragg R-factor R_I, and the weighted Bragg R factor R_{wI}.

The second method of data analysis entailed Rietveld refinement of the entire diffraction profile.[14,15,27,44] Back-
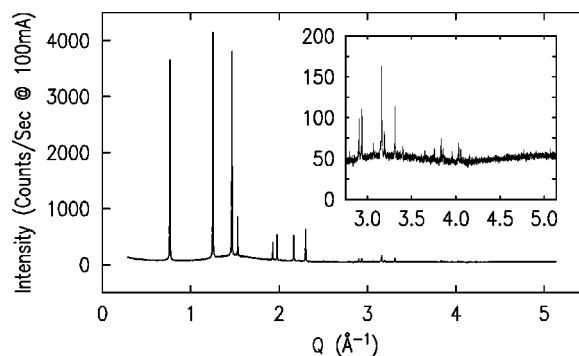

FIG. 2. Room-temperature XRPD pattern for $C_{61}H_2$ cyclopropane collected at NSLS Beamline X3B1. The molecules crystallize on an fcc lattice with a lattice parameter of 14.19 Å. Inset shows the pattern for $2.75 \leq Q \leq 5.13$ Å^{-1} on an expanded scale. The intensity is given in units of counts per second normalized to a synchrotron ring current of 100 mA.

ground diffraction was modeled via linear interpolation between regions far from Bragg peaks. The peak shape employed was an asymmetric Lorentzian. For GSAS refinements, we adopted the framework of the modified Thompson-Cox-Hastings pseudo-Voigt peak-shape function,[42,44] but we typically only refined the relevant parameters associated with the Lorentzian component. It was generally necessary to incorporate a small offset in the "arm zero" setting of the diffractometer, $2\theta_0$, as a variable parameter.

III. ANALYSIS OF THE HIGH-TEMPERATURE STRUCTURE

A characteristic room-temperature XRPD pattern, collected at Beamline X3B1 for $C_{61}H_2$ cyclopropane is shown (after normalization and deadtime correction) in Fig. 2. A LeBail refinement[41,42] established that the lattice is fcc with a cubic lattice parameter of 14.19 ± 0.02 Å .

Two weak non-fcc reflections were observed at $Q = 2.23$ Å^{-1} and $Q = 3.15$ Å^{-1}. Their intensities were on the order of 10–20 counts/sec at a ring current of 100 mA. These features were present in XRPD patterns collected at all temperatures, and were attributed to trace amounts of some non-fullerene impurity. We note that the observed peak positions correspond to the two strongest reflections arising from an fcc NaCl lattice at 299 K. We also observed broad, weak shoulders around the bases of several fcc peaks located near ($Q \sim 1.9 - 2.8$ Å^{-1}). It is likely that these shoulders arise from stacking faults and similar phenomena associated with nonideal crystalline systems that can lead to peak broadening.[14–16,38–40]

Our analysis of the orientationally disordered room temperature structure was similar to that used previously[14,15,21] for the $C_{60}O$ epoxide and 6,5-annulene $C_{61}H_2$. A model of complete spherical disorder can be ruled out on the basis of steric considerations: the van der Waals radius of a fully disordered molecule would be roughly 6.5 Å , which implies that two fully disordered molecules would require a nearest-neighbor distance of *at least* 13 Å .

The incorporation of nearly spherical molecules with attached methylene groups into the fcc lattice can be accom-

plished by requiring that the methylene groups be directed towards the large octahedral voids located along the $\langle 100 \rangle$ axes and/or the smaller tetrahedral voids located along the $\langle 111 \rangle$ axes. Two models for the average molecular structure may be considered: (I) a spherically disordered cage model with variable void occupation and (II) a cylindrically disordered cage model with variable void occupation. In both models, the methylene group can be treated as a single carbon atom, since the contribution to the scattered x-ray intensity arising from the two hydrogen atoms in the methylene group is negligible. In the first case, the central cage is replaced by a spherical shell with the same total charge, while in the second the molecules are cylindrically averaged about the methylene axis, which is then taken to be statistically distributed along the different void directions.

The spherical shell model may appear to be somewhat less physical than the cylindrically disordered model (II) since restrictions on the $C_{61}H_2$ molecular orientation introduced by the methylene group suggest that even the ''average'' cage will not have a truly uniform charge density at all points on the shell. However, this spherically disordered model has the distinct advantage of approximating the librational motion of the cage by incorporating disorder of the shell above and beyond that arising solely from a combination of uniaxial rotation and statistical disorder. Indeed, Vaughan *et al.* found that the high-temperature phase of $C_{60}O$ epoxide was best described using a weighted combination of both the cylindrically disordered and the spherically disordered cage models, although both models independently were also in good agreement with the experimental data and produced similar results.[14,15] We followed the approach of Lommen *et al.*,[21] who adopted the spherically disordered cage model exclusively in their analysis of the high-temperature phase of 6,5-annulene $C_{61}H_2$.

The structure factor for the spherical shell model is obtained by replacing discrete carbon atoms in the C_{60} with a uniform shell of charge. The discrete disorder of the methylene groups is incorporated by placing ''fractional'' methylene groups at positions $\vec{r}_i$ and calculating the Fourier transform, giving

$$S(\vec{Q}) = \frac{60 f_c}{4\pi} \int_0^{2\pi} d\phi \int_{-1}^{1} d(\cos\theta) e^{-iQR_B \cos\theta}$$

$$+ \sum_i \alpha_i f_M e^{i\vec{Q}\cdot\vec{r}_i}$$

$$= 60 f_c j_0(QR_B) + \sum_i \alpha_i f_M e^{i\vec{Q}\cdot\vec{r}_i}, \tag{1}$$

where f_c is the form factor of a carbon atom, R_B is the radius of the carbon shell, f_M is the form factor of a methylene group (typically taken to be identical to the carbon atom form factor), α_i is the probability of finding a methylene group centered at position $\vec{r}_i$, and j_0 is the zeroth order spherical Bessel function.

From the room-temperature XRPD pattern, we extracted 44 integrated intensities using the pattern decomposition procedure outlined in Sec. II. The $\{111\}$ reflection was omitted from our refinement, as discussed above. While the fitted peaks were primarily Lorentzian in nature, the Gaussian
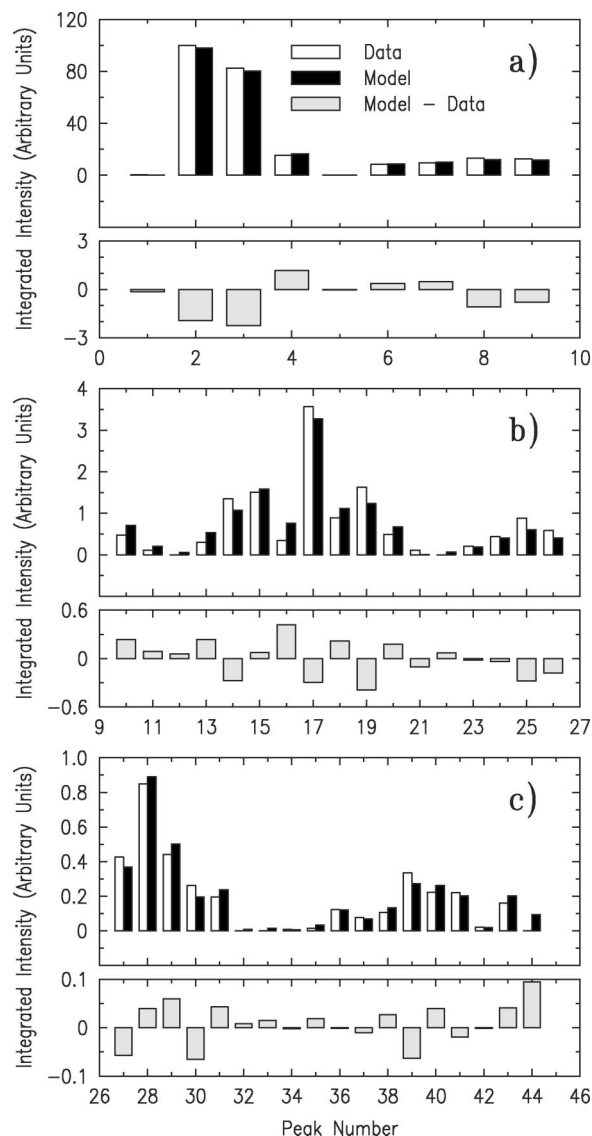

FIG. 3. $C_{61}H_2$ cyclopropane room-temperature refinement: peak integrated intensities, best-fit model, and (model–data) as a function of peak number. Integrated intensities have been scaled to a maximum value of 100.

component of the peaks increased with increasing angle such that the Gaussian fraction f_G varied from ~ 0.0 to ~ 0.4 over the full pattern. The average Lorentzian full width at half maximum (FWHM) was in the range $0.034 \leq \kappa \leq 0.168°$. Four of the 44 integrated intensities at crystallographically allowed positions were indistinguishable from background and were therefore set equal to 0 in the structural refinements.

The complete set of 44 integrated intensities, as shown in Fig. 3, was then fit to the spherical shell model in Eq. (1). For the least-squares fits, the lattice parameter was fixed at the value obtained from our earlier $Fm\bar{3}m$ LeBail refinement. Adjustable parameters included the methylene radius (the distance from the center of the carbon cage to the carbon in the methylene group), the radius of the C_{60} shell, and a single thermal factor for the entire molecule. The addition of a second thermal factor for the methylene carbon was rejected since it was not significant at the 5% confidence level.

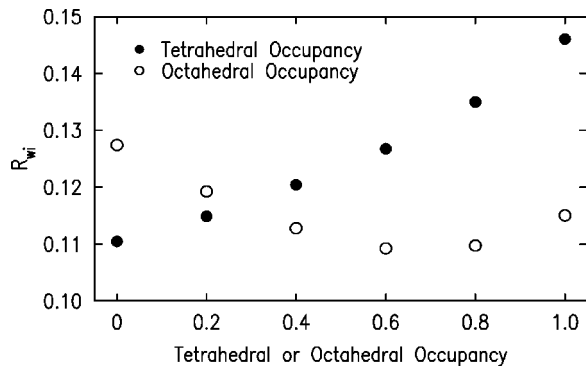To examine the systematics of octahedral and tetrahedral

FIG. 4. Effect of void occupancy on analysis of the room-temperature structure. R_{wI}, the weighted intensity R factor, is plotted as a function of both tetrahedral (filled circles) and octahedral (empty circles) occupancy if *no* constraints are placed on the total number of methylene groups per carbon cage. R_{wI} increases monotonically when the tetrahedral occupancy (filled circles) increases from 0.0 to 1.0 and the octahedral occupancy is allowed to vary. When the octahedral occupancy (empty circles) increases from 0.0 to 1.0 and no constraints are placed on the tetrahedral occupancy, R_{wI} decreases monotonically until reaching a minimum around 0.7.

void occupation, we initially allowed for a variable number of methylene groups per ball resulting in unconstrained octahedral and tetrahedral occupancy parameters α_{oct} and α_{tet}. [So, for example, in Eq. (1), the probability of finding a methylene group in a particular octahedral void would be $\alpha_i = \alpha_{oct}/6$.] Upon increasing the tetrahedral occupancy α_{tet} from 0.0 to 1.0 while allowing the octahedral occupancy to vary, R_{wI} increased monotonically, as shown in Fig. 4. Since the addition of a methylene group into the tetrahedral voids decreased the quality of the fit, the tetrahedral occupancy of the methylene group must be quite small if not identically equal to zero. In addition, when we fixed the tetrahedral occupancy at 0.0, the octahedral occupancy refined to a value of 0.65 as opposed to the ideal value of 1.0. Since the sample contained less than 5% C_{60}, this result is unphysical. When α_{tet} was allowed to vary and α_{oct} was increased from 0.0 to 1.0 (Fig. 4), R_{wI} decreased monotonically until α_{oct} reached a value of roughly 0.5, after which we observed evidence of a broad and shallow minimum centered around 0.7. This

shallow minimum indicates the relative insensitivity of the data to small variations in the octahedral occupancy.

In our final structural refinement, we constrained $\alpha_{oct} + \alpha_{tet} = 1$ so that there was exactly one methylene group per $C_{61}H_2$. Under this assumption, our best refinement yielded $\alpha_{oct} = 0.9 \pm 0.3$ for the octahedral occupancy of the "average" molecule. This is virtually identical to 6,5-annulene $C_{61}H_2$, where the fitted[21] octahedral occupancy was $\alpha_{oct} = 1.0 \pm 0.1$. By contrast, in $C_{60}O$ there is a substantial probability of tetrahedral void occupation,[14,15] with $\alpha_{oct} = 0.66 \pm 0.22$.

The results of our high-temperature integrated intensity refinement are presented in Table I along with previously obtained results on 6,5-annulene $C_{61}H_2$ and $C_{60}O$ epoxide.[14,15,21] Our refinement yielded $\chi^2 = 1.5$, $R_I = 0.05$, and $R_{wI} = 0.12$; these estimates of the goodness or quality of fit all indicate satisfactory agreement between model and data, as shown in Fig. 3, and indicate that this model successfully embodies the key features of the physical system.

The methylene radius refined to a value of 5.0 ± 0.3 Å, to be compared with the oxygen radius[14,15] in $C_{60}O$ of 4.71 Å, and the best-fit $C_{61}H_2$ annulene methylene radius value[21] of 4.9 ± 0.2 Å. The statistically insignificant difference between the methylene radii of the annulene and cyclopropane $C_{61}H_2$ isomers is consistent with the ~ 0.2 Å increase predicted by Curioni *et al.*[28] For the radius of the C_{60} shell, we obtained a best-fit value of $R_B = 3.55 \pm 0.01$ Å. This result agrees with the 6,5-annulene $C_{61}H_2$ fitted shell radius[21] of 3.555 ± 0.007 Å. The rms thermal displacement parameter refined to $\langle u_s \rangle = 0.16 \pm 0.04$ Å, indicating a substantial degree of positional disorder at room temperature.

As seen in Table I, the room-temperature structures adopted by the 6,6-cyclopropane and the 6,5-annulene isomers of $C_{61}H_2$ are both qualitatively and quantitatively similar. Since the refinement of the annulene data used only 26 integrated intensities, as opposed to the 44 used for the cyclopropane refinement, we performed an additional cyclopropane refinement confined to the first 26 integrated intensities. Although $\langle u_s \rangle$ decreased slightly from 0.16 to 0.15 Å and χ^2 increased from 1.5 to 2.7, all refined structural parameters remained unchanged within uncertainty, and no significant changes were observed in either of the integrated intensity R

TABLE I. Comparison of final parameters obtained from $C_{61}H_2$ cyclopropane, $C_{61}H_2$ annulene (Ref. 21), and $C_{60}O$ epoxide (Refs. 14 and 15) room-temperature fits. (Not all parameters were recorded for the epoxide.)

Fitting parameter	$C_{61}H_2$ cyclopropane	$C_{61}H_2$ annulene	$C_{60}O$ epoxide
Lattice parameter	14.19 ± 0.02 Å	14.19 ± 0.02 Å	14.1848 ± 0.0001 Å
Methylene/epoxide radius	5.0 ± 0.3 Å	4.9 ± 0.2 Å	4.71 ± 0.01 Å
C_{60} shell radius	3.55 ± 0.01 Å	3.555 ± 0.007 Å	3.541 Å
Octahedral site occupancy	0.9 ± 0.3	1.0 ± 0.1	0.66 ± 0.22
$\langle u_s \rangle$ of molecule	0.16 ± 0.04 Å	0.12 ± 0.03 Å	
Goodness of fit			
χ^2	1.5	1.2	8.7
R_I	0.05	0.03	
R_{wI}	0.12	0.08	0.15

factors. Thus the obtained results do not depend significantly on the range of data chosen for analysis.

IV. ANALYSIS OF THE LOW-TEMPERATURE STRUCTURE

The crystal structure of 6,6-cyclopropane $C_{61}H_2$ at low temperatures was studied using two data sets: a high-resolution XRPD pattern collected on Beamline X3B1 at $T = 40$ K in the range $0.477 \leq Q \leq 3.740$ Å^{-1}, and a high-statistics XRPD pattern collected on Beamline X7A at 20 K in the range $0.382 \leq Q \leq 6.346$ Å^{-1}. The high-resolution pattern was primarily useful in the determination of the lattice symmetry and parameters, while the high-statistics pattern was most useful in the intensity analysis. Both the room-temperature data presented in Sec. III and the 40-K high-resolution data presented in this section were collected on the same experimental run using the same sample capillary. The 20-K high-statistics data were collected using a second batch of material at a later date.

The high-resolution 40-K powder pattern of the 6,6-cyclopropane isomer of $C_{61}H_2$ was indexed to an orthorhombic unit cell with lattice parameters $a = 13.97$ Å, $b = 14.00$ Å, and $c = 14.25$ Å. Conventional space-group determination was complicated by the nearly degenerate a and b lattice parameters. Although it is possible that the lattice symmetry was higher than primitive orthorhombic, the presence of anomalous profiles (shoulders to peaks that cannot be indexed in an orthorhombic scheme) in the set of peaks in the region $1.94 \leq Q \leq 2.04$ Å^{-1} may indicate a small monoclinic or triclinic distortion of the ideal orthorhombic cell, as well as stacking-fault induced peak shifting and profile distortions similar to those observed in other fullerene systems.[14–16,38–40] As attempts to fit (via LeBail refinement) the pattern to a lower-symmetry monoclinic or triclinic cell failed to reproduce the observed nonorthorhombic shoulders/features, and the key features of the 40-K and 20-K powder patterns are consistent with an orthorhombic unit cell, further analysis was confined to metrically orthorhombic structural models with $P1$ symmetry.

The observation of an orthorhombic structure, rather than the orientationally ordered simple cubic $Pa\bar{3}$ structure adopted by pristine C_{60}, $C_{60}O$ epoxide, and the 6,5-annulene isomer of $C_{61}H_2$, was unexpected. We note that an orthorhombic $Cmca$ unit cell was originally predicted[45] for the low-temperature structure of C_{60}.

The strongest of the two impurity peaks observed in the room-temperature pattern was also visible in the 40-K pattern at $Q = 2.24$ Å^{-1}. The ~ 0.01 Å^{-1} increase in the position of the peak upon cooling from room temperature to 40 K most likely resulted from the thermal contraction of the impurity material. The second weak impurity peak, with an estimated position at 40 K of $Q \approx 3.16$ Å^{-1}, could not be cleanly separated in the analysis from nearby allowed reflections.

The molecular density was clearly constrained from volume considerations to be four molecules per unit cell. Furthermore, from packing considerations, these molecules must be at or close to the face-centered-orthorhombic (or fco) basis sites, although the observation of non-fco reflections in

LeBail fits ruled out the possibility of a true fco phase at low temperatures.

Preliminary estimates of the molecular positions were obtained by treating the molecules as unoriented spherical shells, as in Sec. III, and omitting the methylene group carbons. Using this approach, with the molecules placed on fco sites, we obtained satisfactory agreement with the data for $Q \leq 2.37$ Å^{-1}. The fits were not improved when the molecules were allowed to move away from the fco sites.

It is natural to guess that the methylene groups should be aligned along the longer c axis direction. To explore this question, a second round of fits employed the spherical shell molecule with methylene groups attached. We examined three models: (I) all four methylene groups aligned along the elongated 14.25-Å crystalline c axis; (II) all four methylene groups aligned along the b axis; and (III) all four methylene groups aligned along the a axis. In all cases the orientation and radius of the methylene group were fixed, but the fractional occupancy was varied. Surprisingly, the *poorest* fit ($\chi^2 = 3.63$) was obtained when the methylene axes were aligned with the c axis, and in this case the methylene occupancy refined to a small negative number. Models (II) and (III) yielded more reasonable occupancy values (1.25 and 1.15, respectively) and smaller χ^2 values (3.07 and 3.27). Thus, counterintuitively, these fits suggested that the methylene groups should be aligned along the a and/or b axes.

For more detailed analysis, we performed a Rietveld refinement of the high-statistics 20-K XRPD profile in the range $0.848 \leq Q \leq 4.270$ Å^{-1}, omitting the $2.235 \leq Q \leq 2.272$ Å^{-1} region in the immediate vicinity of the impurity peak, and the low-angle $Q < 0.848$ Å^{-1} data.

Due to the limited number of reflections, it was not possible to refine the positions of all 252 atoms in the unit cell. Therefore our efforts were directed at determining the orientations of the molecules within the unit cell. For the final round of analysis we adopted the *ab initio* pristine C_{60} coordinates obtained by Scuseria[46] along with a methylene group carbon or groups with fractional occupancies. The phase space associated with such a model is still quite large: three Euler angles and three displacement degrees of freedom together with the methylene radius fractional occupancies at different positions for each of four molecules. Although the molecular positions always refined to the fco sites, we quickly found that there were many false minima in χ^2 associated with different choices of the Euler angles. The difficulty is increased if we consider the possibility of minority orientations[2,6–8] similar to those observed in C_{60}. The observation of anomalously large thermal factors ($0.33 \leq \langle u_s \rangle \leq 0.4$ Å) in all the fits to low-temperature data provides a further indication of substantial static and/or dynamic disorder. Clearly, if there are a substantial number of defect orientations or competing crystal structures it will not be possible to reproduce the XRPD pattern with a single crystallographic model.

To define the molecular orientations in any particular model, we began with the molecules in the ''standard orientation,'' in which the molecules occupy the fco sites, with the methylene groups directed along the c axis. The remainder of the molecule was oriented such that the 6:6 carbon-carbon bond bridged by the methylene group was parallel to the crystallographic a axis. From this initial orientation, each
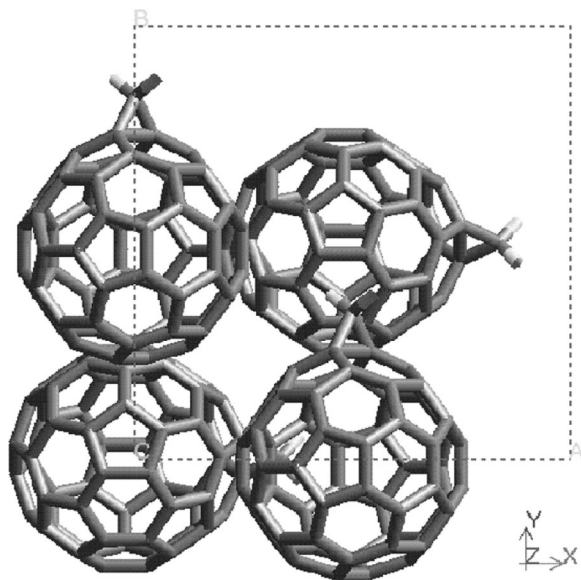
FIG. 5. The unit cell of our best-fit low-temperature $C_{61}H_2$ cyclopropane model in which four molecules occupy the traditional fco basis sites at (000), $(\frac{1}{2}0\frac{1}{2})$, $(\frac{1}{2}\frac{1}{2}0)$, and $(0\frac{1}{2}\frac{1}{2})$. Starting from a configuration in which all molecules are in the standard orientation that aligns the bridgehead 6:6 carbon-carbon bond with the crystallographic a axis, all four molecules are rotated about their methylene axes by $\alpha_{all}=138.6°$ and then rotated about their carbon cage centers by $\beta=90°$. Finally, the molecules at $(\frac{1}{2}0\frac{1}{2})$ and $(0\frac{1}{2}\frac{1}{2})$ are rotated in the plane by $\gamma=90°$, while the molecules at (000) and $(\frac{1}{2}\frac{1}{2}0)$ remain unrotated. In the figure, the methylene group associated with the (000) molecule is directed along the a axis and is thus obscured by the molecule at $(\frac{1}{2}0\frac{1}{2})$.

TABLE II. Best-fit parameter values obtained from the $C_{61}H_2$ cyclopropane 20-K refinement using the structural model illustrated in Fig. 5 along with a disordered spherical shell component. a, b, and c are the lattice parameters of the orthorhombic unit cell. α_{all} is the rotation angle about the methylene axis adopted by all four molecules in the unit cell. η_{dis} refers to the fraction of each molecule which is spherically disordered, while $\langle u_s \rangle$ corresponds to an overall rms isotropic thermal displacement of the molecular center of mass. X, Y, and δ are profile parameters (Refs. 27 and 44) associated with the asymmetric Lorentzian peak shape. χ^2 and the weighted Rietveld R factor, R_{wy} are measures of the goodness of fit.

Fitting parameter	Best-fit value
Lattice parameter a	13.93 ± 0.02 Å
Lattice parameter b	13.98 ± 0.02 Å
Lattice parameter c	14.25 ± 0.02 Å
Carbon cage radius	3.54 Å
α_{all}	138.6°
η_{dis}	0.37
$\langle u_s \rangle$	0.34 Å
X	0.264°
Y	0.0365°
Asymmetry δ	0.94
2θ offset	0.03°
Goodness of fit	
χ^2	66.2
R_{wy}	0.18

molecule was first rotated about the methylene (c) axis by an angle α_i, then rotated about the b axis by an angle β_i, and finally rotated about the c axis by an Euler angle γ_i.

In a large number of different models examined, qualitative agreement with the data was only obtained if the methylene axes were confined to the a-b plane, i.e., *not* along the longer c axis. The result is consistent with that obtained from the simplified spherical shell model, even though in the full-molecule calculations the structure factor was dominated by scattering from the cage carbons rather than the methylene group. Accordingly, all rotations β_i were set equal to $\beta = 90°$.

Motivated in part by the calculations of Harris and Yildirim,[47] and also by the observation that models in which all molecules were aligned along the a axis with different values of α_i did not provide good agreement with the data, we then focused on models incorporating an admixture of a and b methylene axis orientations. We observed that several such in-plane, ''a-b'' models captured key features of the XRPD pattern. We initially tested models in which all rotations α_i were set equal to the same (variable) value α_{all}. When individual angles were allowed to deviate slightly from α_{all} (i.e., different molecules given different angles), it was found that any improvement in the fit was insignificant. Consequently, in the final round of fits we rotated all molecules an angle α_{all} about the c axis, and then all molecules an angle $\beta = 90°$ about the b axis, such that the methylene groups were parallel to the a axis. Each molecule was then

rotated by $\gamma_i = 0$, 90, 180, or 270° about the c axis.

Using this approach, several nearly equivalent minima in χ^2 were found. In our best fit model (Fig. 5), we found $\alpha_{all} = 138.6°$. The molecules at $(\frac{1}{2}0\frac{1}{2})$ and $(0\frac{1}{2}\frac{1}{2})$ are rotated about their carbon cage centers by $\gamma = 90°$ such that their methylene groups are parallel to the b axis, while the molecules at (000) and $(\frac{1}{2}\frac{1}{2}0)$ remain unrotated, with $\gamma = 0°$, leaving their methylene groups aligned with the a axis. The radius of the carbon cage was treated as an adjustable parameter. The methylene radius was held fixed at the room-temperature value of 5.0 Å. The structural model incorporated a disordered spherical shell component in addition to the discrete atoms, and the fraction of ''disordered'' component, η_{dis} was an adjustable parameter. Other adjustable parameters were the Rietveld profile parameters[27,44] δ, X, and Y, an overall scale factor, an rms isotropic thermal displacement factor $\langle u_s \rangle$, three orthorhombic lattice parameters, and a 2θ offset. Attempts to improve on these fits by introducing additional parameters (statistical disorder of the methylene carbons, cylindrical disorder about the methylene axis) resulted in insignificant improvements in χ^2. A summary of the best-fit parameter values derived from the refinement of the low-temperature structural model illustrated in Fig. 5 is presented in Table II.

Figure 6 shows detailed data, model, and difference (model–data) plots covering the fitted portion of the pattern ($0.848 \leq Q \leq 4.270$ Å^{-1}). The overall qualitative agreement between data and model is quite satisfactory. In particular, the model provides a reasonable representation of relative
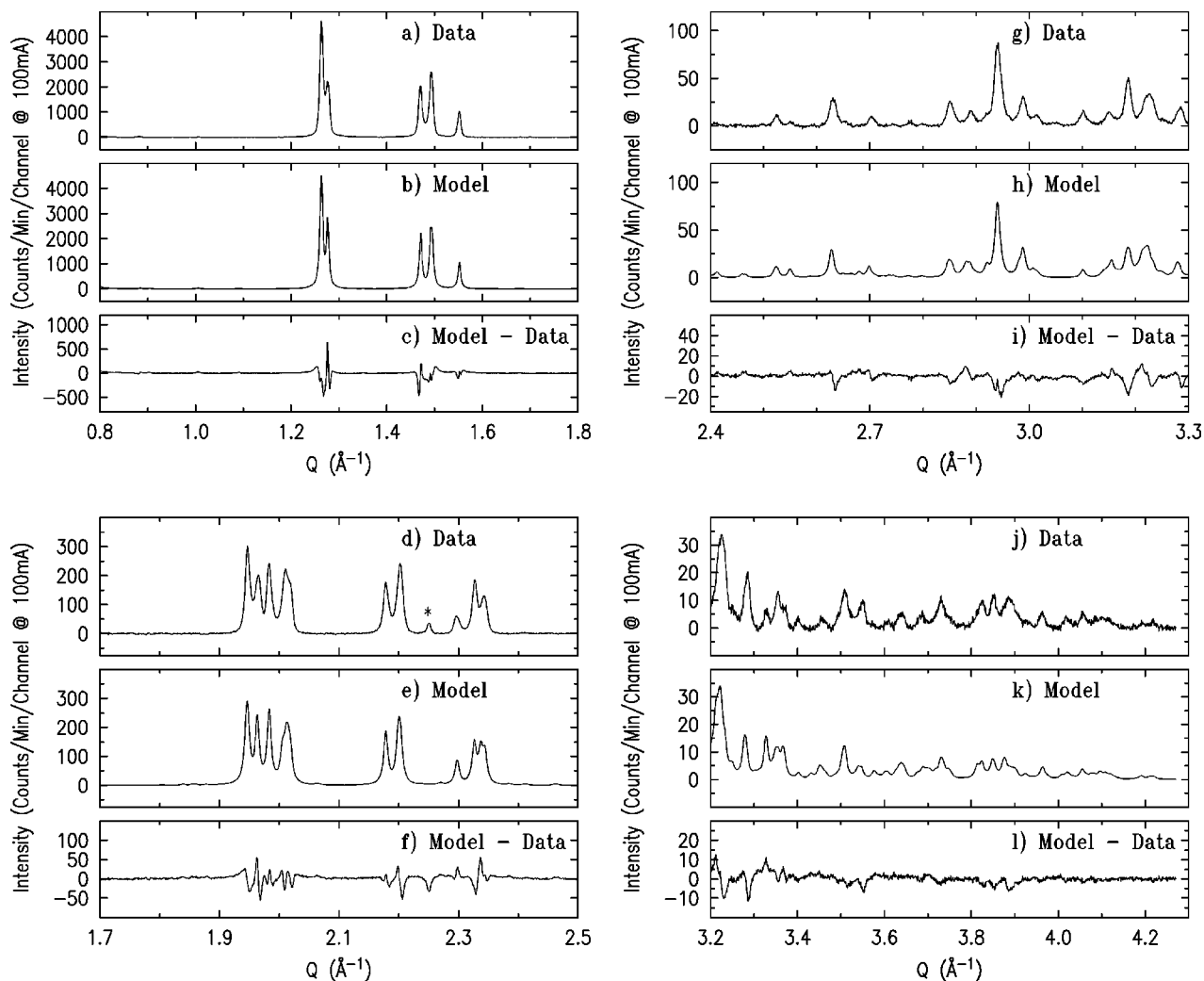
FIG. 6. XRPD data, best-fit model, and (model−data) for $C_{61}H_2$ cyclopropane at 20 K in various ranges of Q. The impurity peak at $Q = 2.24$ Å^{-1} in experimental pattern (d) has been marked with an asterisk.

peak intensities in the $2.4 \leq Q \leq 3.3$ Å^{-1} region, which are primarily influenced by the orientations of the molecules within the unit cell. (We found in the course of examining many models for the molecular orientation that this was the most difficult region to reproduce). The surprisingly poor goodness of fit ($\chi^2 = 66$) most likely arises from limitations in the simplified peak shape used in the refinement, as well as deviations of the linearly interpolated background from the true background.

Although the refinement provided qualitative agreement with much of the XRPD pattern, the quantitative agreement is not at the level normally expected for a true crystallographic refinement. For this reason, we have not attempted to establish error bars for the fitted parameters, except for the lattice parameters, which have an uncertainty of ± 0.02 Å, equal to that associated with the room-temperature cubic lattice parameter. The refined carbon cage radius of 3.54 Å, is in excellent agreement with the room-temperature value of 3.55 ± 0.01 Å. The obtained axial rotation parameter, $\alpha_{all} = 138.6°$, is similar to the 135° angle predicted theoretically by Harris and Yildirim.[47] However, our refinement also suggested that the low-temperature phase incorporates considerable static disorder since refined values of the disordered (spherical) fraction and Debye-Waller parameter were sur-

prisingly large, $\eta_{dis} = 0.37$ and $\langle u_s \rangle = 0.34$ Å.

We made several attempts to model fractional methylene occupancies in the different void directions. We found that neither arbitrary methylene group reversals among the four molecules, nor weighted random occupancy of the voids by methylene groups, led to significant improvements in the fit. In fact, the methylene groups make a relatively small contribution to the entire structure factor. The main discrepancies between the experimental XRPD pattern and the pattern generated by our best-fit model most likely arise from some combination of slightly incorrect cage orientations and, more importantly, the presence of orientational and other defects structures in our sample. Indeed, given the large amount of disorder suggested by our refined values for η_{dis} and $\langle u_s \rangle$, we feel that it is unlikely that any single structure model will reproduce the observed intensities to the level of agreement one typically expects from crystallographic refinements.

V. NATURE OF THE PHASE TRANSITION

The thermal behavior of cyclopropane $C_{61}H_2$ was studied via DSC. Two samples were studied in detail. Sample 1 consisted of 6.3 mg of 6,6-cyclopropane $C_{61}H_2$, loaded into a hermetically sealed aluminum pan under inert argon atmo-
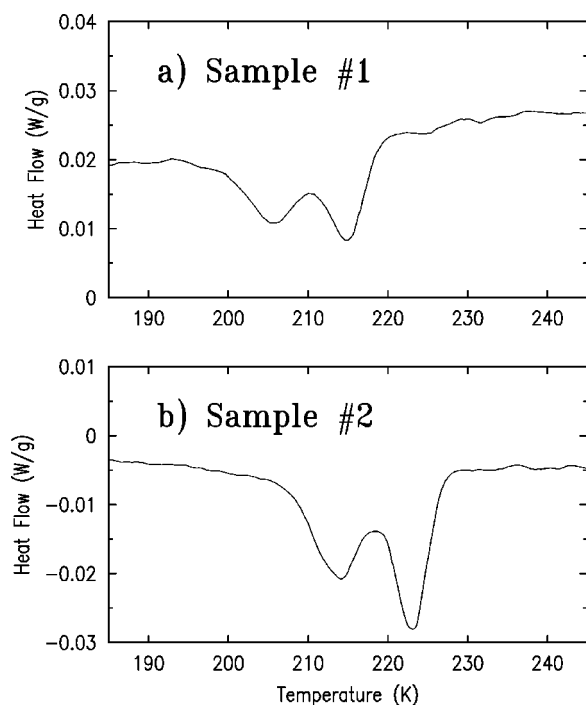
FIG. 7. Differential scanning calorimetry data collected upon heating at 5 K/min for two different samples of $C_{61}H_2$ cyclopropane material. Sample 1 (a) displays transition onset temperatures of 198.6 and 208.1 K and a combined enthalpy change of 2.1 J/g. Sample 2 (b) has onset temperatures approximately 10 K higher (207.8 and 218.2 K, respectively) and a combined enthalpy change of 2.9 J/g.
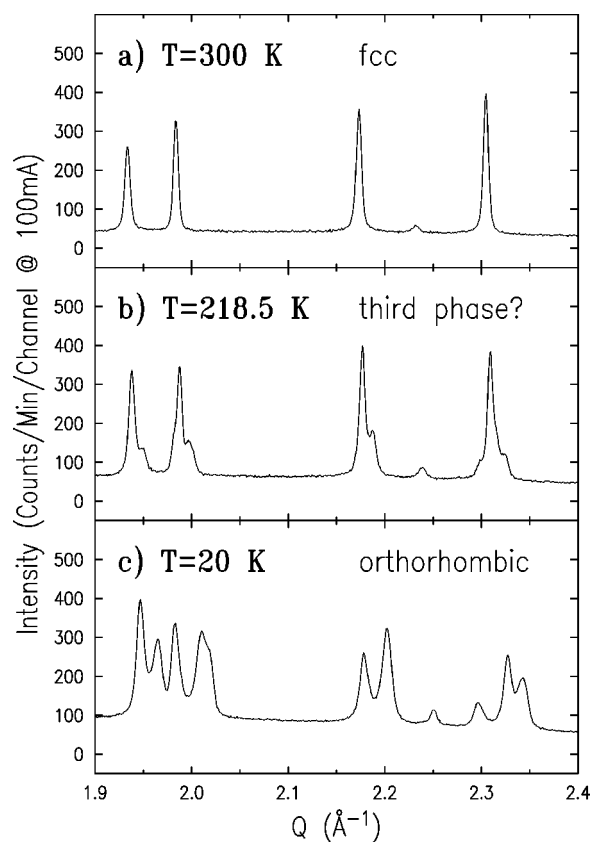

FIG. 8. Representative portions of XRPD patterns for $C_{61}H_2$ cyclopropane sample 2 collected at (a) 300 K (face-centered-cubic), (b) 218.5 K (intermediate), and (c) 20 K (orthorhombic). The weak peak present in all three patterns at $Q \sim 2.24$ Å^{-1} is due to an impurity as discussed in text.

sphere. Sample 2 consisted of 5.2 mg of 6,6-cyclopropane $C_{61}H_2$, loaded in a crimped aluminum pan under air.

Unlike other derivatives of C_{60}, neither sample showed any evidence of a phase transition for $223 \leqslant T \leqslant 373$ K. Scanning calorimetry data are shown in Fig. 7. Sample 1 was first cooled from room temperature to 173 K at 5 K/min and then subsequently held at 173 K for 2 min prior to heating in order to allow for the nucleation of a well-ordered low-temperature phase. Upon heating, we observed *two* slightly overlapping endotherms with onset temperatures of 198.6 and 208.1 K; corresponding enthalpy changes were 1.1 and 1.0 J/g, respectively. The total enthalpy change arising from both transitions was therefore approximately 2.1 J/g for sample 1, which is considerably smaller than the 9.0-J/g enthalpy change associated with the orientational melting transition in the 6,5-annulene isomer of $C_{61}H_2$.

The behavior of sample 2 upon heating was qualitatively similar, although the onset temperatures (207.8 and 218.2 K) were approximately 10 K higher and the associated enthalpy changes (1.4 and 1.5 J/g, respectively) were slightly larger. Presumably, the variations in onset temperatures and transition enthalpies from batch to batch reflect differences in purity with respect to residual solvent, as similar variations have been observed[5] in pristine C_{60}. Indeed, a ^{13}C enriched $C_{61}H_2$ cyclopropane sample prepared for neutron studies exhibited considerably higher onset temperatures of 216.8 and 222.8 K (separated by only 6 K as opposed to 9 or 10 K) upon heating; the combined enthalphy change associated with both transitions was 5.3 J/g (versus 2 or 3 J/g for the first two batches).

The observation of two first-order phase transitions in our calorimetry studies suggests that the orientational melting of solid $C_{61}H_2$ cyclopropane is a two-step process, taking place perhaps via a partially ordered intermediate phase as observed[39] in C_{70}. Therefore an initial guess for the structure of the intermediate phase is one in which the molecules exhibit uniaxial rotation about their methylene axes, resulting in a tetragonal structure. However, analysis of the intermediate phase was complicated by phase coexistence. Since the two phase transitions are separated by only 10 K (to be compared with the 50-K separation observed[39] in solid C_{70}), and the endotherms are typically 6 K wide, multiple phases most likely coexist over the entire "intermediate" phase regime.

Figure 8 shows a representative portion of the XRPD pattern at high temperature, low temperature, and an intermediate temperature $T = 218.5$ K. These data were collected from sample 2. Attempts to index and fit the full 218.5-K pattern to any of a variety of single phase structural models (including a pure tetragonal phase) were unsuccessful. It seems likely that all powder patterns collected at temperatures between the two phase transitions are complicated by the coexistence of two or more phases. When it became clear that a straightforward structural analysis of the intermediate phase would not be possible, we attempted to extract information about the intermediate phase via more indirect methods.

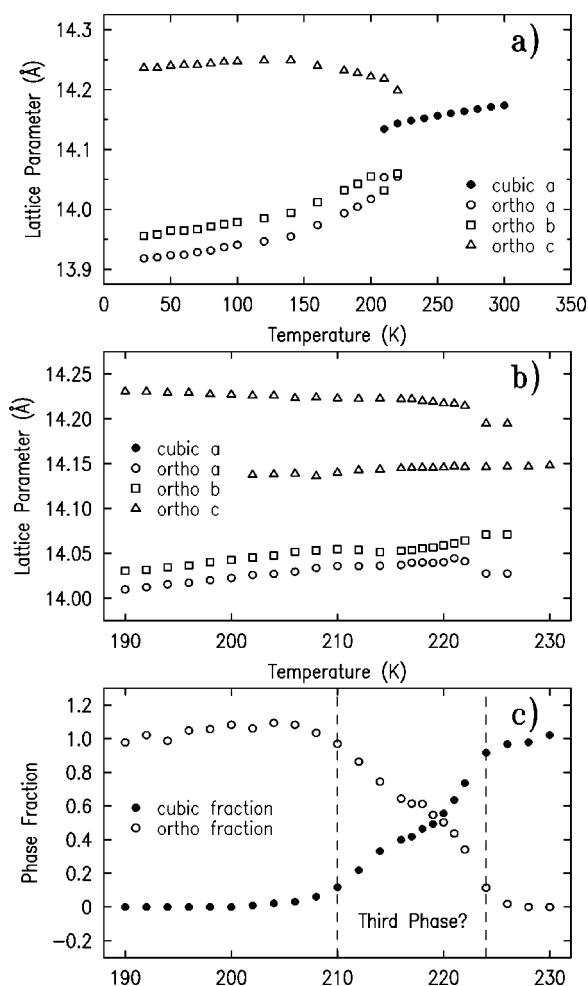One such approach is to make the negative hypothesis

FIG. 9. (a) Lattice parameter values as a function of temperature for both the fcc and orthorhombic phases of $C_{61}H_2$ cyclopropane as determined via LeBail fits, in which all peak intensities were allowed to vary. The open circles, squares, and triangles correspond to the orthorhombic *a*, *b*, and *c* lattice parameters, respectively, while the solid circles correspond to the fcc lattice parameter *a*. (b) Orthorhombic and cubic lattice parameters as a function of temperature for both the fcc and orthorhombic phases of $C_{61}H_2$ cyclopropane determined via fixed intensity ratio fits in the coexistence regime. Note change in temperature scale. (c) Fractional amplitudes of the orthorhombic and fcc phases determined via fixed intensity ratio fits. The temperature regime of the postulated intermediate phase is indicated by vertical dashed lines.

that there is *no* intermediate phase, and to treat the intermediate region as a coexistence of orthorhombic and fcc phases. We performed LeBail fits on 24 powder patterns collected at temperatures between 30 and 300 K, assuming either a pure orthorhombic or fcc phase or a combination of the two. Fits were restricted to the $0.95 < Q < 2.64$ Å^{-1}, and the profile parameters were all held constant in the coexistence region, but the integrated intensity of each peak was allowed to vary. The results of these fits are presented in Fig. 9(a). There are no striking discontinuities in any of the lattice parameters. The apparent convergence of the *a* and *b* orthorhombic lattice parameters between 210 and 220 K will be discussed below.

A second round of fits focused on a slightly smaller portion of the powder pattern, $1.92 < Q < 2.35$ Å^{-1}, in temperatures ranging from 190 to 230 K with 1 or 2 K steps. The patterns at 190 and 230 K were assumed to represent pure orthorhombic and cubic phases, respectively, and we used them to establish best-fit $2\theta_0$ offset, integrated intensity values, profile parameters, and lattice parameters for each of the two pure phases. For each pattern, the fitted integrated intensity values were then divided by the maximum integrated intensity value observed in that pattern, thereby creating a set of characteristic intensity ratios for both the low-temperature orthorhombic phase and the high-temperature fcc phase. Under the assumption that the relative peak intensities and profile parameters for each phase should remain constant throughout the narrow coexistence region, we analyzed the patterns between 190 and 230 K by allowing only the lattice parameters and overall scale factor for each of the two phases to vary [Figs. 9(b) and (c)]. When the analysis was performed in this way, it became clear that the apparent convergence of the *a* and *b* orthorhombic lattice parameters shown in Fig. 9(a) was actually an artifact resulting from the application of the LeBail method, with unrestricted peak intensities, to a weak minority phase.

The fraction of each phase [as shown in Fig. 9(c)] would be expected to display a smooth, S-shaped crossover curve during a single transition between two pure phases. We observed deviations from such ideal behavior in both the cubic phase fraction curve $(210 < T < 220)$ K and the orthorhombic phase fraction curve $(216 < T < 224$ K). This deviation provides additional evidence for the existence of a third, intermediate phase between 210 and 224 K, consistent with the DSC measurements on the same batch of material. In this picture, the onset of 207.8 K for the lower-temperature endotherm corresponds to a first-order transition between the orthorhombic phase and a possibly tetragonal intermediate phase, while the conversion of the intermediate phase to the fcc phase is completed by approximately 227 K.

VI. SUMMARY AND DISCUSSION

We have shown that 6,6-cyclopropane $C_{61}H_2$ exhibits high-temperature behavior similar to that of the 6,5-annulene isomer, with the orientationally disordered molecules crystallizing on an fcc lattice characterized by a lattice parameter of 14.19 Å, such that the methylene groups are statistically disordered among the six equivalent octahedral voids surrounding each molecule. At low temperatures, the $Pa\bar{3}$ structure adopted by the 6,5-annulene isomer is no longer energetically favorable for the 6,6-cyclopropane isomer. Instead, it adopts a low-symmetry orthorhombic structure with lattice parameters (at 20 K) $a = 13.93$ Å, $b = 13.98$ Å, and $c = 14.25$ Å. Although one would expect the molecules in such a structure to align their methylene axes with the longer crystallographic *c* axis, our structural analysis strongly suggests that the methylene groups are directed toward some combination of octahedral voids in the *a-b* plane. In particular, we propose a simple model in which the methylene groups of molecules at (000) and $(\frac{1}{2}\frac{1}{2}0)$ occupy *a* octahedral voids while those of molecules at $(\frac{1}{2}0\frac{1}{2})$ and $(0\frac{1}{2}\frac{1}{2})$ occupy *b* octahedral voids. This model leads to excellent qualitative agreement with the 20-K XRPD pattern upon the refinement of α_{all}, a single rotation angle about the methylene axis for

all four molecules. The low-temperature phase is also characterized by considerable static disorder, most likely arising from orientational and other defects.

The 6,6-cyclopropane $C_{61}H_2$ is the ''least perturbed'' C_{60} derivative observed to deviate significantly from the characteristic solid-state behavior of pristine C_{60}. Thus it sets a lower bound on the degree of perturbation required to induce non-C_{60} behavior. In $C_{60}O$ epoxide and $C_{61}H_2$ annulene, the phase behavior is altered quantitatively, but not qualitatively, from that of pristine C_{60}. By contrast, when the cyclopropane $C_{61}H_2$ cooled from room temperature, the methylene groups at the 6,6 positions act somehow to prevent the cubic $Pa\overline{3}$ phase from forming. This could take place either because the methylene groups project slightly farther into the voids, or because the 6:6 bonds are not directed as close to voids as the 6:5 bonds, so that an unacceptable distortion of the structure would be required in order to enable all methylenes to reside in voids. In any case, with the $Pa\overline{3}$ phase effectively eliminated by a combination of steric and symmetry constraints, the temperature must drop considerably before another, orthorhombic, crystal structure becomes thermodynamically favorable. However, detailed calculations at the atomic level, using realistic potentials, will be required to establish all the factors that stabilize the orthorhombic structure.

Orientational melting appears to be a two-step process, with an intermediate phase strongly indicated by calorimetry and supported by a detailed analysis of the powder diffraction profiles. The transitions are broadened sufficiently that there is most likely phase coexistence throughout the transition region. Further advances in our understanding of both the low-temperature structure and the nature of the phase transition will most likely require the preparation of solvent-free single crystals, which would represent a challenging materials processing project.

ACKNOWLEDGMENTS

---

*Present address: Department of Physics, University of Waterloo, Waterloo, Ontario, Canada N2L 3G1.

†Corresponding author.

‡Present address: Laboratory of Crystallography, Universität Bayreuth, D-95440 Bayreuth, Germany.

§Present address: Symmorphix Inc., 1278 Reamwood Avenue, Sunnyvale, CA 94089.

**Present address: Department of Chemistry, Louisiana State University, Baton Rouge, Louisiana 70803.

[1] R. M. Fleming, T. Siegris, P. M. Marsh, B. Hessen, A. R. Kortan, D. W. Murphy, R. C. Haddon, R. Tycko, G. Dabbagh, A. M. Mujsce, M. L. Kaplan, and S. M. Zahurak, in *Clusters and Cluster-Assembled Materials*, edited by R. S. Averback, J. Bernholc, and D. L. Nelson, MRS Symposium Proceedings (Materials Research Society, Pittsburgh, 1991), p. 691.

[2] P. A. Heiney, J. E. Fischer, A. R. McGhie, W. J. Romanow, A. M. Denenstein, J. P. McCauley, Jr., A. B. Smith III, and D. E. Cox, Phys. Rev. Lett. **66**, 2911 (1991).

[3] R. Sachidanandam and A. B. Harris, Phys. Rev. Lett. **67**, 1467 (1991).

[4] W. I. F. David, R. M. Ibberson, J. C. Matthewman, K. Prassides, T. J. S. Dennis, J. P. Hare, H. W. Kroto, R. Taylor, and D. R. M. Walton, Nature (London) **353**, 147 (1991).

[5] P. A. Heiney, J. Phys. Chem. Solids **53**, 1333 (1992).

[6] J. R. D. Copley, D. A. Neumann, R. L. Cappelletti, W. A. Kamitakahara, E. Prince, N. Coustel, J. P. McCauley, Jr., N. C. Maliszewskyj, J. E. Fischer, A. B. Smith III, K. M. Creegan, and D. M. Cox, Physica B **180&181**, 706 (1992).

[7] W. I. F. David, R. M. Ibberson, T. J. S. Dennis, J. P. Hare, and K. Prassides, Europhys. Lett. **18**, 219 (1992).

[8] R. Hu, T. Egami, F. Li, and J. S. Lannin, Phys. Rev. B **45**, 9517 (1992).

[9] P. Launois, S. Ravi, and R. Moret, Int. J. Mod. Phys. B **13**, 253 (1999).

[10] J. E. Fischer and P. A. Heiney, J. Phys. Chem. Solids **54**, 1725 (1993).

[11] M. Sprik, A. Cheng, and M. L. Klein, J. Phys. Chem. **96**, 2027 (1992).

[12] J. P. Lu, X. Li, and R. M. Martin, Phys. Rev. Lett. **68**, 1551 (1992).

[13] K. M. Creegan, J. L. Robbins, W. K. Robbins, J. M. Millar, R. D. Sherwood, P. J. Tindall, D. M. Cox, A. B. Smith III, J. P. McCauley, Jr., D. R. Jones, and R. T. Gallagher, J. Am. Chem. Soc. **114**, 1103 (1992).

[14] G. B. M. Vaughan, P. A. Heiney, D. E. Cox, A. R. McGhie, D. R. Jones, R. M. Strongin, M. A. Cichy, and A. B. Smith III, Chem. Phys. **168**, 185 (1992).

[15] G. B. M. Vaughan, Ph.D. thesis, University of Pennsylvania, 1993.

[16] S. van Smaalen, R. E. Dinnebier, I. Holleman, G. von Helden, and G. Meijer, Phys. Rev. B **57**, 6321 (1998).

[17] S. van Smallen, R. E. Dinnebier, W. Schnelle, I. Holleman, G. von Helden, and G. Meijer, Europhys. Lett. **43**, 302 (1998).

[18] T. Suzuki, Q. Li, K. C. Khemani, and F. Wudl, J. Am. Chem. Soc. **114**, 7301 (1992).

[19] A. B. Smith III, R. M. Strongin, L. Brard, G. T. Furst, and W. J. Romanow, J. Am. Chem. Soc. **115**, 5829 (1993).

[20] A. B. Smith III, R. M. Strongin, L. Brard, G. T. Furst, W. J. Romanow, K. G. Owens, R. J. Goldschmidt, and R. C. King, J. Am. Chem. Soc. **117**, 5492 (1995).

[21] A. N. Lommen, P. A. Heiney, G. B. M. Vaughan, P. W. Stephens, D. Liu, D. Li, A. L. Smith, A. R. McGhie, R. M. Strongin, L. Brard, and A. B. Smith III, Phys. Rev. B **49**, 12 572 (1994).

[22] D. A. Neumann, J. E. Fischer, J. R. D. Copley, P. A. Heiney, J. J. Rush, R. M. Strongin, L. Brard, and A. B. Smith III, in *Science and Technology of Fullerene Materials*, MRS Symposium Proceedings No. 359, edited by P. Bernier, T. W. Ebbesen, D. S. Bethune, R. M. Metzger, L. Y. Chiang, and J. W. Mintmire (Materials Research Society, Pittsburgh, 1995), p. 537.

[23] D. A. Neumann, Q. Huang, J. R. D. Copley, J. E. Fischer, P. A. Heiney, R. M. Strongin, L. Brard, and A. B. Smith III, in *Recent*

Advances in the Chemistry and Physics of Fullerenes and Related Materials, edited by R. S. Ruoff and K. M. Kadish (The Electrochemical Society, Pennington, NJ, 1995), p. 791.

[24] C. Meingast, G. Roth, L. Pintschovius, R. H. Michel, C. Stoermer, M. M. Kappes, P. A. Heiney, L. Brard, R. M. Strongin, and A. B. Smith III, Phys. Rev. B **54**, 124 (1996).

[25] J. M. Hawkins, A. Meyer, T. A. Lewis, S. Loren, and F. J. Hollander, Science **252**, 312 (1991).

[26] R. Taylor and R. M. Walton, Nature (London) **363**, 685 (1993).

[27] M. R. Stetzer, Ph.D. thesis, University of Pennsylvania, 2000.

[28] A. Curioni, P. Giannozzi, J. Hutter, and W. Andreoni, J. Phys. Chem. **99**, 4008 (1995).

[29] R. M. Fleming, A. R. Kortan, B. Hessen, T. Siegrist, F. A. Thiel, P. Marsh, R. C. Haddon, R. Tycko, G. Dabbagh, M. L. Kaplan, and A. M. Mujsce, Phys. Rev. B **44**, 888 (1991).

[30] A. K. Gangopadhyay, J. S. Schilling, M. De Leo, W. E. Buhro, K. Robinson, and T. Kowalewski, Solid State Commun. **96**, 597 (1995).

[31] R. Céolin, V. Agafanov, B. Bachet, A. Gonthier-Vassal, H. Szwarc, S. Toscani, G. Keller, C. Fabre, and A. Rassat, Chem. Phys. Lett. **244**, 100 (1995).

[32] J. M. Hawkins, T. A. Lewis, S. D. Loren, A. Meyer, J. R. Heath, R. J. Saykally, and F. J. Hollander, J. Chem. Soc. Chem. Commun. **991**, 775 (1991).

[33] G. B. M. Vaughan, P. A. Heiney, J. E. Fischer, D. E. Luzzi, D. A. Ricketts-Foot, A. R. McGhie, Y.-W. Hui, A. L. Smith, D. E. Cox, W. J. Romanow, B. H. Allen, N. Coustel, J. P. McCauley, Jr., and A. B. Smith III, Science **254**, 1350 (1991).

[34] W. W. Wendlandt, in *Thermal Analysis*, Chemical Analysis, Vol. 19, 3rd ed., edited by P. J. Elving and J. D. Winefordner (John Wiley & Sons, New York, 1986).

[35] M. A. Brown, *Introduction to Thermal Analysis* (Chapman and Hall, New York, 1988).

[36] B. Wunderlich, *Thermal Analysis* (Academic Press, New York, 1990).

[37] D. E. Cox, in *Synchrotron Radiation Crystallography* (Academic Press, New York, 1992), Chap. 9.

[38] R. Berliner and S. A. Werner, Phys. Rev. B **34**, 3586 (1986).

[39] G. B. M. Vaughan, P. A. Heiney, D. E. Cox, J. E. Fischer, A. R. McGhie, A. L. Smith, R. M. Strongin, M. A. Cichy, and A. B. Smith III, Chem. Phys. **178**, 599 (1993).

[40] G. B. M. Vaughan, Y. Chabre, and D. Dubois, Europhys. Lett. **31**, 525 (1995).

[41] A. LeBail, H. Duroy, and J. L. Fourquet, Mater. Res. Bull. **23**, 447 (1988).

[42] A. C. Larson and R. B. Von Dreele, *GSAS*: *General Structure Analysis System*, Los Alamos National Laboratory Report No. LAUR 86-748, 1994 (unpublished). GSAS can be obtained from ftp://ftp.lanl.gov/public/gsas

[43] P. R. Bevington and D. K. Robinson, *Data Reduction and Error Analysis for the Physical Sciences*, 2nd ed. (WCB/McGraw-Hill, New York, 1992).

[44] R. A. Young, in *The Rietveld Method*, International Union of Crystallography Monographs on Crystallography, Vol. 5, edited by R. A. Young (Oxford University Press, New York, 1996), Chap. 1.

[45] Y. Guo, N. Karasawa, and W. A. Goddard III, Nature (London) **351**, 464 (1991).

[46] G. E. Scuseria, Chem. Phys. Lett. **176**, 423 (1991).

[47] T. Yildirim and A. B. Harris (unpublished).